## Title

Noninvasive wearable electroactive pharmaceutical monitoring for personalized therapeutics



## Journal

Proceedings of the National Academy of Sciences of the United States of America, 117(32)

## ISSN

0027-8424

## Authors

Lin, Shuyu
Yu, Wenzhuo
Wang, Bo
et al.

## Publication Date

2020-08-11

## DOI

10.1073/pnas.2009979117

Peer reviewed

# Noninvasive wearable electroactive pharmaceutical monitoring for personalized therapeutics

Shuyu Lin[a], Wenzhuo Yu[a], Bo Wang[a], Yichao Zhao[a,b], Ke En[a,b], Jialun Zhu[a,b], Xuanbing Cheng[a,b], Crystal Zhou[a,c], Haisong Lin[a], Zhaoqing Wang[a], Hannaneh Hojaiji[a], Christopher Yeung[a,b], Carlos Milla[d], Ronald W. Davis[e,1], and Sam Emaminejad[a,f,1]

[a]Interconnected & Integrated Bioelectronics Lab (I[2]BL), Department of Electrical and Computer Engineering, University of California, Los Angeles, CA 90095; [b]Department of Materials Science and Engineering, University of California, Los Angeles, CA 90095; [c]Department Physiology, University of California, Los Angeles, CA 90095; [d]The Stanford Cystic Fibrosis Center, Center for Excellence in Pulmonary Biology, Stanford School of Medicine, Stanford, CA 94305; [e]Stanford Genome Technology Center, Stanford School of Medicine, Palo Alto, CA 94304; and [f]Department of Bioengineering, University of California, Los Angeles, CA 90095

Contributed by Ronald W. Davis, June 18, 2020 (sent for review May 19, 2020; reviewed by John S. Foster and David R. Hillyard)

**To achieve the mission of personalized medicine, centering on delivering the right drug to the right patient at the right dose, therapeutic drug monitoring solutions are necessary. In that regard, wearable biosensing technologies, capable of tracking drug pharmacokinetics in noninvasively retrievable biofluids (e.g., sweat), play a critical role, because they can be deployed at a large scale to monitor the individuals' drug transcourse profiles (semi) continuously and longitudinally. To this end, voltammetry-based sensing modalities are suitable, as in principle they can detect and quantify electroactive drugs on the basis of the target's redox signature. However, the target's redox signature in complex biofluid matrices can be confounded by the immediate biofouling effects and distorted/buried by the interfering voltammetric responses of endogenous electroactive species. Here, we devise a wearable voltammetric sensor development strategy—centering on engineering the molecule–surface interactions—to simultaneously mitigate biofouling and create an "undistorted potential window" within which the target drug's voltammetric response is dominant and interference is eliminated. To inform its clinical utility, our strategy was adopted to track the temporal profile of circulating acetaminophen (a widely used analgesic and antipyretic) in saliva and sweat, using a surface-modified boron-doped diamond sensing interface (cross-validated with laboratory-based assays, $R^2 \sim 0.94$). Through integration of the engineered sensing interface within a custom-developed smartwatch, and augmentation with a dedicated analytical framework (for redox peak extraction), we realized a wearable solution to seamlessly render drug readouts with minute-level temporal resolution. Leveraging this solution, we demonstrated the pharmacokinetic correlation and significance of sweat readings.**

personalized pharmacotherapy | therapeutic drug monitoring | wearable sensors | pharmacokinetics | surface engineering

To realize the vision of personalized medicine, which aims to deliver the right drug to the right patient at the right dose, personalized pharmacotherapy solutions are necessary (1, 2). Currently, medication dosage is generally prescribed by relying on the drug manufacturer's recommendation, which is based on statistical averages obtained from testing the medication on a relatively small patient sample size (3, 4). Therefore, at the individual level the prescribed dosage may fall outside the optimal therapeutic concentration window, resulting in adverse events in patients and/or ineffective pharmacotherapy (5, 6). To address such issues, personalized therapeutic drug monitoring (TDM) is essential, as it can guide dosing by capturing the dynamic pharmacokinetic profile of the patient's prescribed medication during the course of the treatment (7–10). However, because of the invasiveness, high cost, and long turnaround time of the available TDM techniques (mostly relying on repeated blood draws and assays performed in off-site central laboratories), they are applied on rare occasions and at suboptimal rates (11, 12).

In that regard, wearable and mobile biochemical sensing technologies capable of analyzing noninvasively retrievable biofluids are suitable solutions, because they can potentially be deployed at a large scale to monitor individuals' drug pharmacokinetic profiles (semi)continuously and longitudinally (13–18). Specifically, in the context of biofluids such as sweat and saliva, the free (unbound) drug molecules are speculated to diffuse into the secreted biofluids with high degrees of correlation with blood (owing to their low molecular weight, less than a few kilodaltons) (19, 20). Therefore, in principle, these noninvasive sensing modalities can be adopted to provide proxy measures of target drug concentration in blood (Fig. 1*A*).

Accordingly, sensor development strategies are required to render sample-to-answer drug detection capabilities within a compact footprint. In that regard, voltammetry-based approaches have been introduced to target electroactive drugs which do not rely on recognition elements (21, 22). These approaches transduce the target's redox chemical signature into a

## Significance

To achieve the mission of personalized medicine, centering on delivering the right drug to the right patient at the right dose, therapeutic drug monitoring solutions are necessary. By devising a surface engineering strategy, we created a voltammetric sensing interface, featuring an "undistorted potential window," within which the target electroactive drug's voltammetric response is dominant and interference is eliminated, rendering reliable target quantification in noninvasively retrievable biofluids (sweat and saliva). Leveraging this sensing interface, a fully integrated, wearable solution was constructed to seamlessly render drug readouts with minute-level temporal resolution. To inform its clinical utility, the solution was utilized to demonstrate noninvasive pharmacokinetic monitoring of a pharmaceutical (here, acetaminophen, a widely used analgesic and antipyretic) in a wearable format.

Author contributions: S.L., R.W.D., and S.E. designed research; S.L., W.Y., B.W., Y.Z., K.E., J.Z., X.C., C.Z., H.L., Z.W., and H.H. performed research; S.L., W.Y., B.W., Y.Z., K.E., J.Z., X.C., C.Z., H.L., Z.W., H.H., and S.E. contributed new reagents/analytic tools; S.L., W.Y., B.W., Y.Z., K.E., J.Z., X.C., C.Z., H.L., Z.W., H.H., C.Y., C.M., R.W.D., and S.E. analyzed data; and S.L. and S.E. wrote the paper.

Reviewers: J.S.F., Owl Biomedical; and D.R.H., University of Utah School of Medicine.

The authors declare no competing interest.



[1]To whom correspondence may be addressed. Email: katrina.hong@stanford.edu or emaminejad@ucla.edu.

This article contains supporting information online at https://www.pnas.org/lookup/suppl/doi:10.1073/pnas.2009979117/-/DCSupplemental.

First published July 27, 2020.

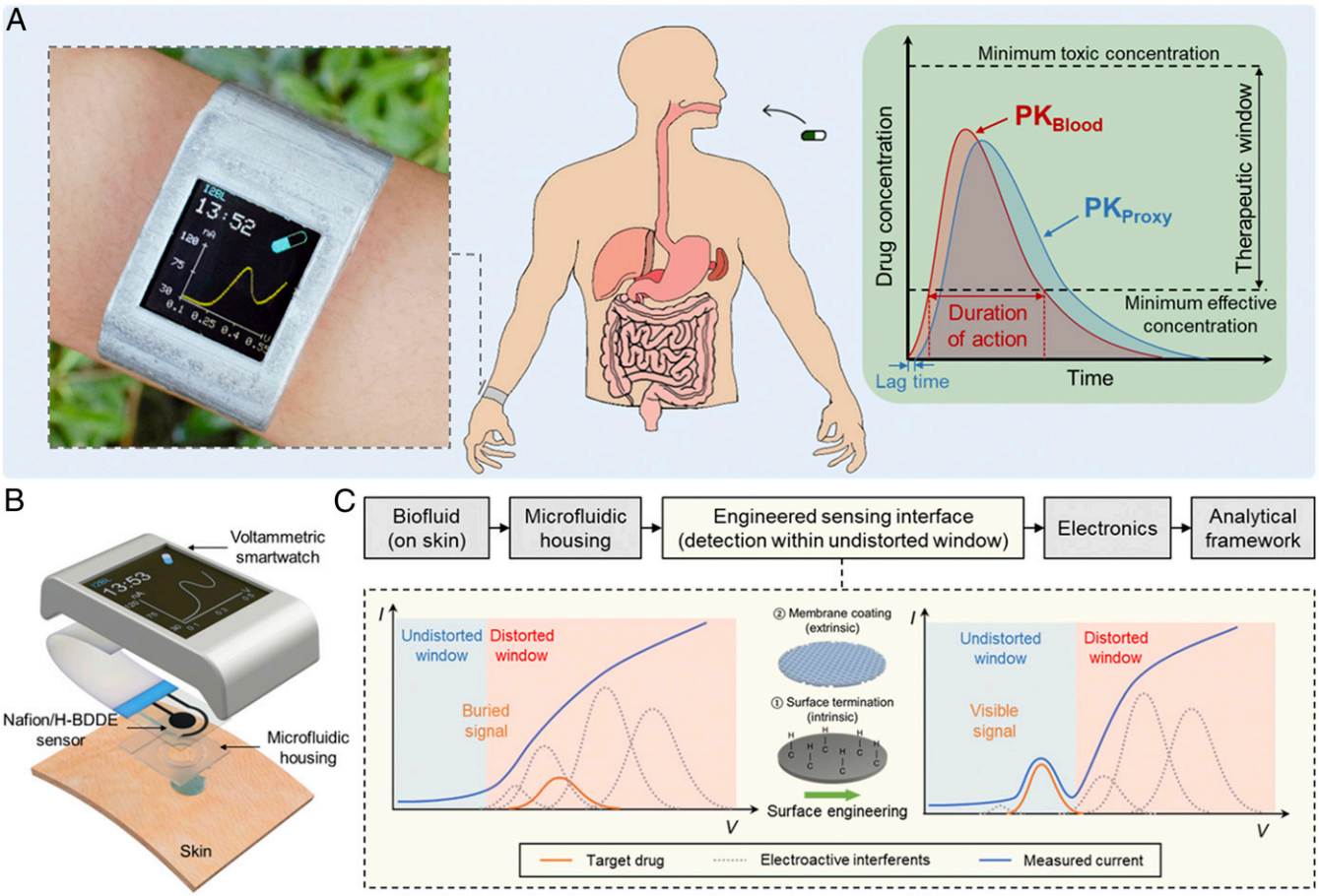


**Fig. 1.** A fully integrated, wearable voltammetric drug monitoring solution: design rationale and application. (*A*) A voltammetric smartwatch, which can be applied to track the circulating drug's pharmacokinetics (PK) by providing proxy readouts in noninvasively retrievable biofluids. (*B*) An illustrative exploded view of the smartwatch components (containing microfluidic housing, Nafion/H-BDDE sensor, signal processing/transmission circuitry, LCD screen, and battery units, all embedded within a 3D-printed case). (*C*) Seamless operational workflow of the devised wearable voltammetric drug monitoring solution, utilizing an engineered voltammetric sensing interface to create an undistorted potential window for target drug detection (in the presence of endogenous electroactive interferents).

measurable electrical signal using millimeter-sized sensing electrodes. To adapt such approaches for the envisioned translational applications, the fundamental challenges inherent to complex biofluid analysis must be addressed.

One such challenge is the distortion/burial of the target's redox signature in the measured voltammogram, which is due to superimposing voltammetric responses of endogenous electroactive species ("interference"). As reported in our previous work, the characterization of the electroactive interferent species' response led to the identification of "undistorted potential windows," within which reliable electroactive target detection in sweat matrix was demonstrated (22). To generalize this methodology and apply it to the targets with redox peaks falling outside the original undistorted potential windows, surface engineering strategies are needed to tune the target/interference surface interactions such that the target redox peaks fall within the undistorted potential windows. Additionally, biofouling is another challenge relevant to the context at hand, which is widely investigated for the conventional biofluids (e.g., blood) (23, 24) but overlooked in the context of sweat analysis. Biofouling stems from the adsorption of surface-active agents (e.g., proteins, peptides, and amino acids) onto the sensor's surface (25, 26). This adsorption layer inhibits the analyte interaction with the electrode, which may lead to signal degradation.

Here, to resolve the aforementioned challenges, we devise a wearable voltammetric sensor development strategy that centers on tuning the molecule–surface interactions. We specifically tailored our strategy to target acetaminophen (APAP) as a model electroactive drug molecule with a reported saliva–blood correlation (27, 28); APAP is a widely used analgesic and antipyretic, and its supratherapeutic administration is the leading cause of liver failure in the United States (29). To engineer an APAP-sensing interface, the surface termination of the working electrode was adjusted to decouple the undesired interference (via tuning the electron transfer kinetics pertaining to redox reactions), and a polymeric membrane was incorporated to reject surface-active agents (also, to further reject undesired interference). These orthogonal intrinsic/extrinsic surface treatments converged to the development of a Nafion-coated and hydrogen-terminated boron-doped diamond electrode (Nafion/H-BDDE), which simultaneously mitigates biofouling and creates undistorted potential windows encompassing the APAP's oxidation peak. Using this engineered sensing interface, accurate and reliable quantification of APAP in saliva and sweat was realized (cross-validated with laboratory-based assays, $R^2 \sim 0.94$).

To realize a wearable solution, the engineered sensing interface was integrated within a custom-developed smartwatch (capable of sweat sampling/routing, signal acquisition, and data display/transmission), where the voltammetric readouts were processed by

a dedicated analytical framework for target redox peak extraction (Fig. 1 *B* and *C*). To illustrate its clinical utility, we applied this wearable solution to construct the pharmacokinetic profile of APAP in sweat (in relation to saliva) and accordingly demonstrated the significance of sweat-based drug readings. By harnessing the demonstrated real-time and reliable drug quantification capabilities, our generalizable solution can be positioned as a viable TDM approach to enable personalized pharmacotherapy.

## Results

Here, to quantify the target electroactive drug molecule, we selected differential pulse voltammetry (DPV), because of its ability to suppress nonfaradaic background current (30). To reliably measure the APAP's voltammetric response in biofluids with complex matrices, its redox peak should fall within the "undistorted potential windows," defined as potential ranges within which the voltammetric contributions of interfering species are negligible. In the previously reported comprehensive interference study of biofluids (such as sweat), uric acid (UA), tyrosine (Tyr), and tryptophan (Trp) have been particularly identified as major endogenous contributors to the measured voltammogram of the sweat matrix (over the potential range of 0 to 1 V) (22). Therefore, in this work we first focused on systematically characterizing their voltammetric responses in relation to that of the APAP, in order to guide our sensor development efforts.

The voltammetric responses of electroactive species are controlled by the electron transfer kinetics of their corresponding redox reactions at the sensor surface, which are represented by parameters such as electron transfer rate constant and the redox species' surface concentrations (30, 31). By modulating these parameters—via tuning the sensing electrode's surface properties (e.g., surface polarity or morphology)—the reactions of concerns can be selectively accelerated or suppressed (32, 33). Thus, through elaborate surface engineering, we can decouple the voltammetric response of the target from that of the interferents, such that the target redox peak(s) fall within the undistorted potential window(s) (33–36).

To construct the sensing interface, we used a BDDE as the working electrode, because of its wide electrochemical potential window, low background current, intrinsically high biofouling resistance, and high operational stability (22, 37–39). The surface chemistry of the BDDE can be tuned by adjusting its surface termination (effectively, altering the BDDE's surface states), an attribute that can be exploited as a degree of freedom for tuning the reaction kinetics of various analytes. Examples of BDDE termination include hydrogen and oxygen termination, which were previously exploited for the electroanalysis of electroactive species (40). Accordingly, here we used as-deposited BDDE, with default hydrogen termination, and we performed anodic treatment on BDDE to achieve oxygen termination (37).

Our voltammetric characterization of the selected interferents (UA, Tyr, and Trp, performed individually) in phosphate-buffered saline (PBS), using an oxygen-terminated BDDE (O-BDDE), informed an undistorted potential window spanning from 0 to 0.3 V. The voltammetric characterization of APAP, using the same interface, yielded an oxidation peak location at ∼0.65 V, which overlaps with the oxidation peaks of all three interferents (Fig. 2*A*). The same characterization experiments were performed using a hydrogen-terminated BDDE (H-BDDE), the results of which are illustrated in Fig. 2*B*. As compared to the O-BDDE case, the H-BDDE–measured oxidation peak of APAP was shifted to a less positive potential relative to Tyr and Trp, informing the decoupling of the interference of Tyr and Trp. However, this surface termination change also leads to the shift of UA's oxidation peak to a lower potential, which overlaps with that of APAP. It is worth noting that the larger response and the lower oxidation potential of APAP indicates its higher electron transfer rate on H-BDDE (41). This observation is aligned with previously reported characterizations of APAP oxidation (42, 43) and may be attributed to the enhancement in the interaction of APAP and reduced-carbon surface (44).

To eliminate the interfering voltammetric response of UA, a surface modification step was incorporated in our surface engineering approach, as an additional measure, orthogonal to the devised surface termination adjustment. Noting that UA is predominantly present in its negatively charged form (urates) in physiologically relevant pH (given its dissociation constant, $pK_a$, = 5.6) and APAP is electrically neutral, here we selected a negatively charged permselective membrane to repel urates from approaching the sensing surface. Specifically, we chose Nafion, because it features negatively charged sulfonate groups in its polymer chain and it was demonstrated to possess antifouling effects (45, 46). As shown in Fig. 2*C*, the voltammetric response of UA, measured by a Nafion/H-BDDE, was significantly suppressed, leading to the widening of the undistorted potential window. Given that this widened window encompasses APAP's oxidation peak, it can be concluded that the detection of APAP will be minimally influenced by all of the model interferents.

To verify our surface engineering rationale, the voltammograms of 10 μM APAP solutions (in PBS) were obtained and compared with those of 10 μM APAP solutions spiked with model interferents (within their physiologically relevant concentration). As shown in Fig. 2 *D* and *E*, the measured voltammograms by the bare O-BDDE and H-BDDE illustrated that the oxidation peaks of APAP were buried and distorted after the introduction of the interferents, respectively. However, the use of the devised Nafion/H-BDDE led to a well-distinguishable APAP voltammetric response (as evident from the undistorted oxidation peak; Fig. 2*F*). To further validate the suitability of Nafion/H-BDDE for the selective detection of APAP, we characterized the interference of other endogenous electroactive species (within their physiologically relevant concentration range in biofluid, e.g. sweat). As shown in *SI Appendix*, Fig. S1, the introduction of histidine, methionine, or ascorbic acid into the APAP solutions did not distort the oxidation response of APAP. Overall, the results from this comprehensive interference study are in agreement with our surface engineering rationale and illustrate the utility of the devised strategy.

The devised Nafion/H-BDDE interface can also be leveraged to mitigate biofouling, a critical constraint overlooked by the previously reported wearable sensors but widely investigated in the direct electroanalysis of conventional biofluids (e.g., blood). To illustrate the severity of this issue in our context, we characterized the biofouling effect occurring in the sweat matrix. We particularly used an iontophoretically induced sweat sample, spiked with 10 μM of APAP, as a target medium.

Accordingly, first the biofouling of a conventional carbon electrode (screen-printed carbon electrode, SPCE) was characterized via tracking the changes to the voltammetric response in the sweat sample (measured repeatedly over time). Because each voltammetric scan consumes a negligible amount of analyte (31), the analyte amount in the sample stays the same, and thus the sequentially recorded redox peak levels are expected to remain unchanged. As shown in Fig. 2*G*, although the SPCE-measured APAP oxidation presented an obvious peak in the buffer matrix (*SI Appendix*, Fig. S2*A*), its voltammetric signal in the sweat matrix was merely a weak bump, which disappeared completely within three scans. This signal degradation can be attributed to the immediate and progressive adsorptions of the surface-active agents present in sweat, which inhibit the electron transfer of target electroactive molecules [in line with previously reported conclusions made in the context of the analysis of other biofluids (24)]. Therefore, the observed rapid (three scans performed over ∼5 min) and total sensor response degradation illustrates that the sensing interface is unsuitable for the envisioned application.

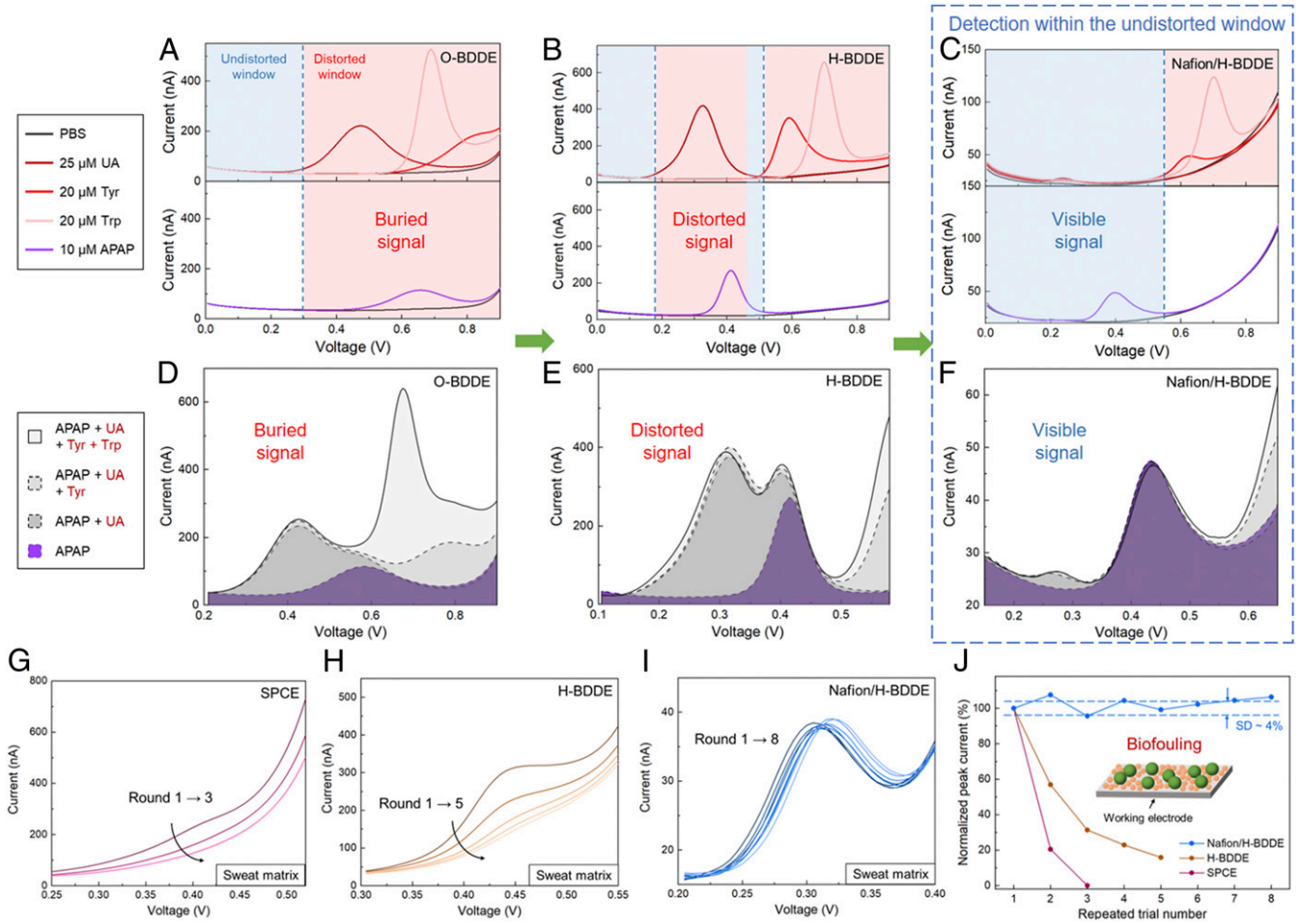


**Fig. 2.** Engineering a voltammetric sensing interface for APAP detection within a created undistorted potential window with a high biofouling resistance. (*A–C*) Characterization of the individual DPV response of the selected endogenous electroactive interferents and the target (with respect to the electrochemical background) using O-BDDE (*A*), H-BDDE (*B*), and Nafion/H-BDDE (*C*) sensors. (*Upper*) Twenty-five micromolar UA, 20 μM Tyr, 20 μM Trp. (*Lower*) Ten micromolar APAP. The interferents' potential windows of influence (distorted windows) and the undistorted windows are annotated. (*D–F*) Characterization of the DPV response of the target in presence of interferents (all at the same concentration levels as stated above) using O-BDDE (*D*), H-BDDE (*E*), and Nafion/H-BDDE (*F*) sensors. (*G–I*) Sequentially recorded differential pulse voltammograms of a sweat sample (spiked with 10 μM APAP) on SPCE (*G*), H-BDDE (*H*), and Nafion/H-BDDE (*I*) interfaces. (*J*) Corresponding voltammetric peak current of the spiked-sweat measurements (extracted with the aid of the analytical framework). The values are normalized with respect to those obtained in the corresponding first rounds. (*Inset*) The schematic of biofouling.

Next, we repeated the same biofouling characterization procedure using a bare BDDE (specifically, H-BDDE; see *SI Appendix*, Fig. S2*B* and Fig. 2*H*). The results indicate the presence of biofouling-induced signal degradation, although it occurred at a lower rate than the case of the SPCE (as evident from the distinguishable response after five repeated measurements). It is worth noting that the observed relatively low signal degradation rate is in line with one of our motivations for choosing the BDDE: leveraging the BDDE's intrinsically high biofouling resistance (due to the weak adsorption of polar molecules of its $sp^3$-carbon structure) (38, 47). Given that the biofouling-induced signal degradation needs to be further mitigated for reliable sensing, we investigated whether the antifouling effect of the Nafion membrane can be harnessed. Accordingly, we performed the same characterization study with a Nafion/H-BDDE (*SI Appendix*, Fig. S2*C* and Fig. 2*I*), where minimal signal degradation was observed over the course of eight consecutive measurements. The biofouling characterization results, collectively, indicate that the Nafion/H-BDDE presents considerably superior performance in comparison to the SPCE and H-BDDE (Fig. 2*J*) in terms of the preservation of the sensing fidelity in biofluid matrices.

The demonstrated APAP detection capabilities (in complex matrices) of the devised Nafion/H-BDDE sensing interface can be leveraged to reliably quantify APAP in noninvasively retrievable biofluids. To illustrate this point, we first used the Nafion/H-BDDE to monitor the voltammetric response of APAP in saliva and sweat samples, which were spiked with known amounts of APAP to construct samples with concentrations spanning from 1 μM to 100 μM (corresponding to the physiologically relevant range). Specifically, the saliva samples were collected by passive drool, and the sweat samples were collected following the standard iontophoresis protocol (48), both from healthy human subjects without recent APAP administration histories. Fig. 3 *A* and *B* show the corresponding recorded voltammograms of the saliva and sweat samples. To extract the APAP oxidation peak information from the voltammograms, baseline estimation and correction were performed (*SI Appendix*, Fig. S3) with the aid of a dedicated analytical framework [following our previously reported methodology (22)]. For the case of both biofluids, a linear relationship between the measured/extracted voltammetric peak currents and the APAP concentration levels were observed (Fig. 3 *A* and *B*, *Inset*; $R^2$ = 0.97 and 0.99 for saliva and sweat measurements, respectively),

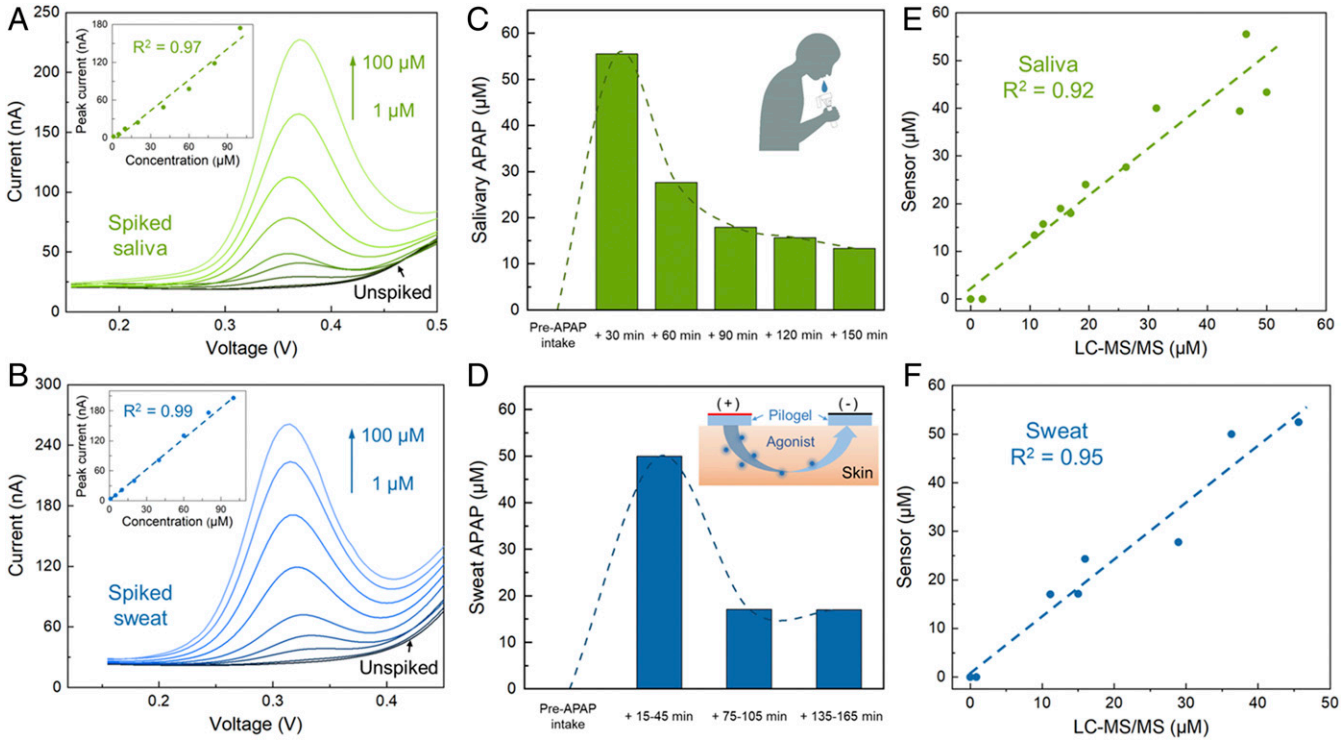


**Fig. 3.** Nafion/H-BDDE-enabled ex situ APAP quantification in noninvasively retrieved biofluid samples of (*A*, *C*, and *E*) saliva and (*B*, *D*, and *F*) sweat. (*A* and *B*) Differential pulse voltammograms of unspiked and spiked (with 1, 5, 10, 20, 40, 60, 80, and 100 μM APAP) saliva (*A*) and sweat (*B*) samples. (*Insets*) The corresponding analytical framework-extracted peak current. (*C* and *D*) Sensor-measured APAP concentration in the saliva (*C*) and sweat (*D*) samples of a human subject, collected before and at intermittent time points after the oral administration of a medication containing 650 mg APAP. (*Insets*) The schematics of saliva collection and iontophoresis-based sweat stimulation. (*E* and *F*) Sensor-measured APAP concentrations in saliva (*E*) and sweat (*F*) samples versus the corresponding LC-MS/MS readouts.

with a limit of detection of 1 μM. It is also noteworthy that the voltammograms recorded in both unspiked saliva and sweat samples do not exhibit any redox peak, demonstrating the minimal voltammetric influence of endogenous electroactive interferents (in line with our conclusions from the interference study).

To demonstrate the clinical utility of the sensing interface, the Nafion/H-BDDE was applied to track the temporal profile of circulating APAP in individuals taking APAP-based medication. Accordingly, following the aforementioned biofluid collection procedure, saliva and sweat samples were obtained from two subjects before and at intermittent time points after their regularly scheduled medication administration (containing 650 mg APAP). The obtained saliva and sweat samples were analyzed by the Nafion/H-BDDE sensors and the corresponding voltammograms were processed with the aid of the analytical framework. Fig. 3 *C* and *D* show the postcalibrated concentration profiles of APAP in the saliva and sweat samples of the first subject (the corresponding results for subject 2 are shown in *SI Appendix*, Fig. S4). Based on the sensor readouts, no APAP was detected in the saliva and sweat prior to medication intake, and a rapid increase, followed by a gradual elimination, of APAP was observed upon intake (for both subjects). The captured trends are similar to the previously reported APAP pharmacokinetic profiles (27). Furthermore, the measured APAP concentrations in sweat and saliva samples were cross-validated via laboratory instrument measurements (using liquid chromatography with tandem mass spectrometry (49), LC-MS/MS, with the calibration curve in *SI Appendix*, Fig. S5). As shown in Fig. 3 *E* and *F*, the sensor-estimated APAP concentrations closely matched the LC-MS/MS readouts ($R^2 = 0.92$ and 0.95 for saliva and sweat, respectively). These results, collectively, indicate that the devised voltammetric sensing interface can accurately measure APAP in noninvasively retrievable biofluids and can be positioned to track the temporal profile of circulating APAP.

The demonstrated sensor's high accuracy in capturing the temporal profile of circulating APAP in sweat motivated the positioning of the sensor for pharmacokinetic monitoring applications. To this end, we developed and validated an integrated wearable solution to seamlessly measure the APAP's dynamic level in real time (Fig. 4*A*). Accordingly, the engineered voltammetric sensor was integrated within a custom-developed smartwatch, which consists of 1) a microfluidic interface (consisting of sweat sampling and sensing chambers), 2) a Nafion/H-BDDE–based voltammetric sensing interface for APAP quantification, and 3) an electronic interface (Fig. 4*B* and *SI Appendix*, Fig. S6) for DPV-based signal excitation/acquisition and data display/transmission (via a liquid-crystal display and a wireless Bluetooth module, respectively). To map the smartwatch-based readouts to the corresponding APAP concentration levels, the redox feature was extracted from the measured voltammograms by the dedicated analytical framework (similar to the ex situ saliva and sweat study above).

Specifically, to enable efficient sweat sampling and real-time analysis, a skin-adhesive thin-film microfluidic interface was developed (constructed by vertical integration of tape-based layers with laser-cut patterns), which features low-volume sweat collection and sensing chambers (50). To characterize the microfluidic interface's sweat sampling function, an assembled microfluidic device was placed on the iontophoretically stimulated skin surface of a human subject (in which case, the sensor was replaced by a transparent plastic film to allow for visualization). As shown in *SI Appendix*, Fig. S7, in this trial the sensing chamber became fully filled in less than 3 min after the initiation of the sweat

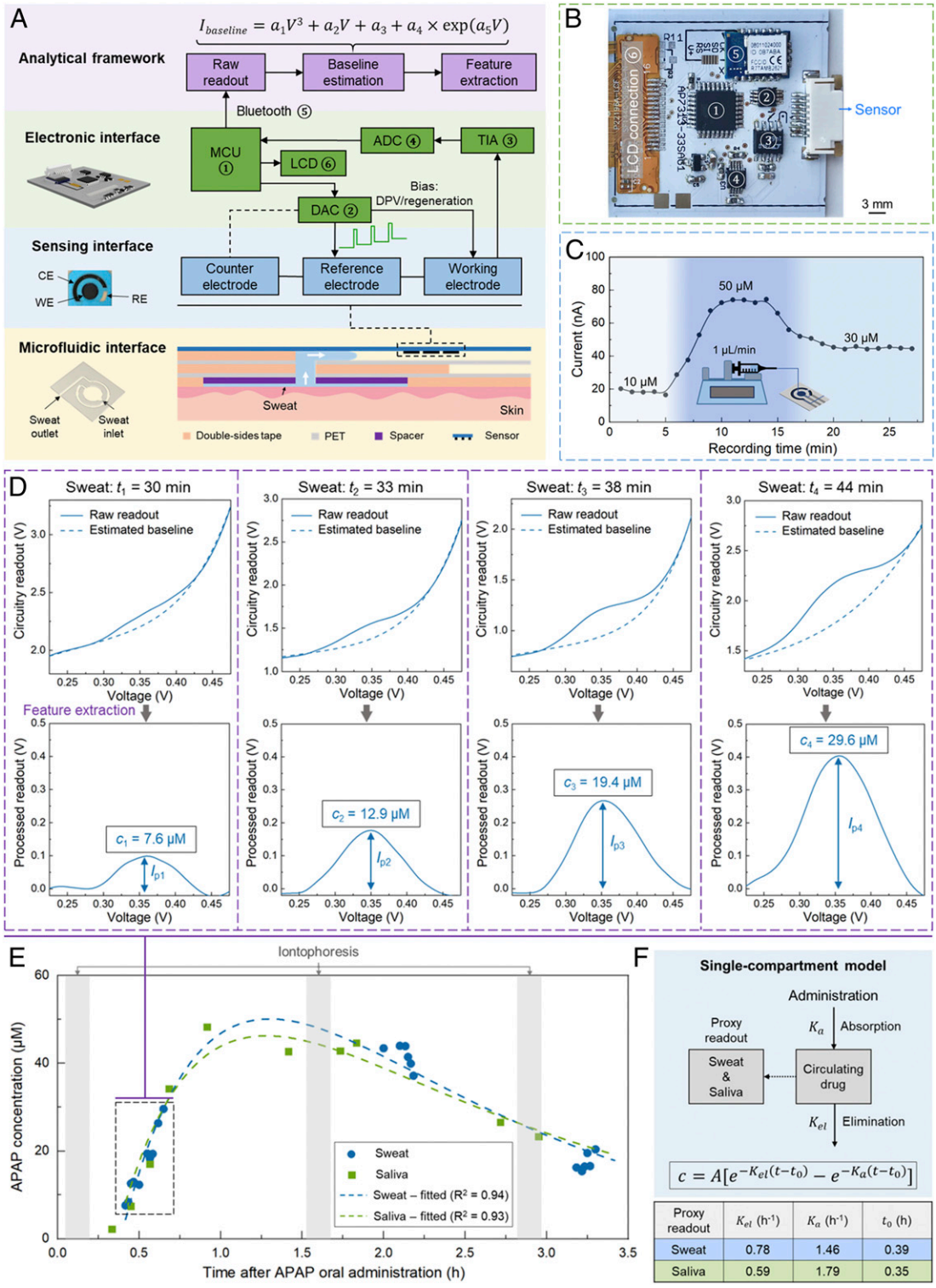


| Proxy readout | $K_{el}$ ($h^{-1}$) | $K_a$ ($h^{-1}$) | $t_0$ (h) |
|---|---|---|---|
| Sweat | 0.78 | 1.46 | 0.39 |
| Saliva | 0.59 | 1.79 | 0.35 |

**Fig. 4.** A Nafion/H-BDDE-enabled wearable solution for on-body pharmacokinetic monitoring. (*A*) System-level block diagram of the developed wearable solution, consisting of microfluidic, sensing, and electronic interfaces, and an analytical framework. The top-view photo of the Nafion/H-BDDE-based sensor illustrates the footprint of the working (3.6-mm diameter), counter, and reference electrodes (WE, CE, and RE) used. (*B*) Photo of the custom-developed wireless DPV readout circuit board, which integrates commercially available electronic components, including 1) an MCU, 2) a DAC, 3) a TIA, 4) an ADC, 5) a Bluetooth transceiver module, and 6) a thin-film-transistor LCD screen. (*C*) Sensor's response to solutions with varying APAP concentration levels, where the APAP solutions were introduced by a continuous flow setup (*Inset*). Peak current values were extracted using the analytical framework. (*D*) The captured and processed differential pulse voltammograms of sweat (performed by the wearable solution), corresponding to four representative time points. (*Top*) Raw measurements and estimated baselines (*Bottom*). Baseline-corrected voltammograms to derive the APAP levels. (*E*) The measured APAP concentration levels in sweat and saliva versus time after oral administration of APAP. Each of the measurement series were fitted into a single-compartment pharmacokinetic model. (*F*) Schematic of the applied single-compartment model and the tabulated pharmacokinetic parameters, which were extracted from the APAP readouts shown in *E*.

secretion, demonstrating the capability of the microfluidic interface to sample fresh sweat with minute-level temporal resolution.

To evaluate the devised solution's ability to track the dynamically varying drug concentration levels, the sensor was embedded in the microfluidic sensing chamber and connected to a continuous-flow system delivering APAP solutions with varying concentration levels (Fig. 4 *C*, *Inset*). Specifically, 10, 50, and 30 μM APAP (in PBS) solutions were consecutively delivered, with the aid of a programmable syringe pump, at 1 μL/min (similar level to the sweat secretion rate, induced by the standard iontophoresis procedure). To ensure high signal reproducibility in this setting, a cathodic electrical pulse (0.5 s, −0.4 V) was applied between the DPV scans [which has been shown to mitigate the potential carryover effects in continuous measurements (51, 52)]. As shown in Fig. 4*C*, the measured APAP peak current levels tracked the increase and subsequent decrease of the APAP concentration in the introduced solutions, and in all three concentration cases, stable peak current measurements were obtained.

The integrated wearable solution was then applied to seamlessly track the APAP's pharmacokinetic profile in sweat and investigate its sweat–saliva correlation. Accordingly, a volunteer subject with prescheduled APAP medication intake was recruited. To access sweat throughout the expected time window of the drug's circulation, standard iontophoresis was performed at intermittent time points, and after each stimulation the sensing system was mounted on the stimulated area to perform in situ sweat sampling and analysis. To assess the sweat–saliva correlation, saliva samples were obtained intermittently during the experiment.

During the course of the sweat secretion, DPV scans were performed consecutively. The raw DPV readouts (by the circuit) and corresponding APAP oxidation peaks (extracted by the analytical framework) at four representative time points are shown in Fig. 4*D*. The collected saliva samples were analyzed in parallel using the developed sensors. The collective readouts are shown in Fig. 4*E*, which indicates that the captured APAP trend in sweat mirrors the trend in saliva: both feature distinct absorption and elimination phases with similar temporal characteristics. To quantitatively compare these characteristics in sweat versus saliva, the captured concentration readouts were curve-fitted following the single-compartment model (53):

$$c = A\left[e^{-K_{el}(t-t_0)} - e^{-K_a(t-t_0)}\right], \quad [1]$$

where $t$ is time after the oral administration of the APAP, $t_0$ is the lag time (with respect to the administration time, effectively the total lag time of oral administration→blood and blood→-sweat/saliva drug partitioning), $A$ is the preexponential factor, and $K_{el}$ and $K_a$ are the elimination and absorption rate constants, respectively (Fig. 4*F*). The extracted pharmacokinetic parameters in saliva are similar to the previously reported saliva-based analysis (54). Moreover, the resemblance of the fitted pharmacokinetic profiles of sweat and saliva (fitted curve in Fig. 4*E*) and the similarity of their extracted parameters (tabulated in Fig. 4*F*) suggest a potentially high degree of sweat–saliva correlation. Given the readily established saliva–blood correlation of APAP (27), the results from our study support the potential clinical utility of sweat for noninvasive TDM.

## Discussion and Outlook

We demonstrated a fully integrated wearable solution for seamless TDM (targeting APAP as a model drug), which centers on engineering a voltammetric sensing interface for reliable electroactive drug analysis in biofluid matrices. We first performed interference and biofouling characterization studies to identify the key analytical constraints and guide our voltammetric sensor development efforts. In order to resolve the identified constraints, we devised a surface engineering strategy to selectively tune target/interference-surface interactions via 1) modulating the intrinsic surface properties (by adjusting the surface termination) and 2) incorporating an extrinsic permselective membrane. By employing these orthogonal intrinsic/extrinsic surface treatment approaches, we realized a Nafion/H-BDDE sensing interface, which simultaneously mitigates biofouling and creates an undistorted potential window for APAP detection. Leveraging this interface, we demonstrated accurate APAP quantification in both sweat and saliva (cross-validated with laboratory-based assays, $R^2 \sim 0.94$).

To render seamless APAP readouts on-body, we integrated the engineered sensing interface into a custom-developed smartwatch, which was coupled with a dedicated analytical framework for voltammetric readout processing. By applying this solution in a human subject study, we captured the APAP's pharmacokinetic profile in sweat and saliva. Of particular interest is the similarity of the APAP's dynamic profile in both matrices (in terms of concentration level and absorption/elimination kinetics), suggesting a similar analyte partitioning mechanism from blood. These results inform the potential clinical utility of sweat as a TDM matrix, motivating further clinical investigations toward establishing its utility.

This study demonstrates the pharmacokinetic correlation and significance of sweat readings, enabled by devising a thin microfluidic-based sensing system capable of rendering accurate and minute-level drug readouts in sweat. The presented surface engineering strategy can be adapted, with minimal reconfiguration, toward the quantification of a wide panel of electroactive endogenous and exogenous molecules. Toward expanding our drug monitoring capabilities, other sensing mechanisms (e.g., affinity-based) can also be explored to target nonelectroactive drugs. It is noteworthy that targeting drugs with narrow therapeutic concentration windows is of particular clinical interest, because real-time monitoring can be harnessed to enable timely intervention and prevent adverse outcomes such as drug toxicity. To this end, the inclusion of auxiliary sensing interfaces to characterize the sweat-related matrices, such as sweat rate, sweat pH (with respect to the drug's $pK_a$), and body hydration, can be helpful to account for the inter/intraindividual drug partitioning variations. Furthermore, large-scale clinical studies need to be performed to construct the drugs' sweat–blood correlation and establish sweat-based pharmacokinetic profiles, in which case the application of data analytics techniques can be particularly useful to improve the accuracy of the drugs' proxy readouts. In that regard, the results from saliva-based studies can serve as suitable references to guide the engineering and clinical efforts.

The convergence of these efforts will establish a noninvasive and real-time TDM modality, which allows the collection of longitudinal patient-specific datasets at large scale. Harnessing these unprecedented capabilities can enable new patient-centric pharmacotherapy solutions (including drug compliance/abuse monitoring, personalized drug dosing, and feedback-controlled drug delivery), and can create new dimensions to direct drug and treatment development efforts.

## Materials and Methods

**Materials and Reagents.** APAP, UA, L-tyrosine, L-tryptophan, ascorbic acid, L-methionine, L-histidine, Nafion perfluorinated resin solution (5 wt %), and APAP-$D_4$ solution (100 μg/mL in methanol) were purchased from Sigma-Aldrich. PBS (1×, pH 7.2; Gibco), isopropyl alcohol, and all of the reagents used in the high-performance liquid chromatography (HPLC) were purchased from Fisher Scientific. Polyethylene terephthalate (PET, 100 μm thick) was purchased from MG Chemicals. Double-sided tape (170 μm thick, 9474LE 300LSE) and Scotch single-sided self-seal laminating sheets were purchased from 3M Science. BDDE sensor (reference electrode: silver; counter electrode: carbon) was purchased from Metrohm USA. SPCE (TE100) was purchased from CH Instruments Inc.

**Electrode Preparation and Electrochemical Measurements.** The electrochemical measurements were performed using a CHI660E electrochemical workstation (CH Instruments, Inc.). To alter the BDDE surface from H termination to O termination, anodic treatment was performed in an electrochemical cell (+2 V vs. silver/silver chloride, Ag/AgCl, for 5 min) containing 0.5 M sulfuric acid ($H_2SO_4$). Electrochemical cleaning of BDDE was performed by cyclic voltammetry (CV) each time before use in 0.5 M $H_2SO_4$. Accordingly, for H-BDDE, the CV scanning was performed in the potential range of −0.5 V to 1.5 V (vs. Ag/AgCl; scan rate: 0.5 V/s, 10 cycles). For O-BDDE, a CV scanning range of −0.5 V to 2.8 V was used. Nafion coating was performed by drop-casting 1.8 μL 5 wt % Nafion solution onto the working electrode, followed by drying in the ambient environment.

DPV measurements were performed with increment: 5 mV, amplitude: 50 mV, pulse width: 0.1 s, sampling width: 16.7 ms, pulse period: 0.5 s. In continuous DPV measurements, given the unidirectional nature of the applied DPV potential waveform (here, only scanning within the oxidation reaction range without a cyclic renewal), progressive analyte depletion and product buildup can occur. Accordingly, a constant potential of −0.4 V was applied across the working and reference electrodes for 0.5 s before each DPV scan. In the characterization of the biofouling effect, the peak current levels from the measurements were extracted using the analytical framework.

**Sweat and Saliva Collection and Ex Situ Measurement.** For sweat stimulation and collection, a standard iontophoresis protocol was followed using the Macroduct Sweat Collection System (ELITechGroup Inc.). First, the volar surface of the human subject's forearm was cleaned with isopropyl alcohol and deionized water. Next, 5-min iontophoresis was performed using the pilocarpine-loaded hydrogels and a Webster sweat inducer. The secreted sweat was then collected with the Macroduct sweat collector for 30 min. To track the circulating temporal profile of APAP in sweat, iontophoresis was performed four times, at ∼1 h before and ∼10 min, ∼70 min, and ∼130 min after the oral administration of a medication containing 650 mg APAP (Regular Strength Pain Relief; CVS Health). Saliva samples were collected by direct salivation into plastic vials with the aid of the Saliva Collection Aid (Salimetrics). The subjects were instructed to rinse their mouths with cold water before saliva collection. To track the circulating temporal profile of APAP in saliva, saliva samples were collected before and 30, 60, 90, 120, and 150 min after the APAP administration. Collected sweat and saliva samples were stored at −20 °C before use.

Saliva samples were centrifuged at 14,000 × *g* for 10 min before performing measurements. To quantify APAP concentration in the samples, 40 μL of the sweat/saliva sample was drop-cast onto the sensor, followed by the DPV scanning. To calibrate the DPV readout, the respective APAP-less sweat or saliva sample (prior to the medication administration, from the same subject) was spiked with 1 mM APAP stock solution (in PBS) to construct a 50 μM calibrator. The peak current from the calibrator (measured after the real samples) was used to calibrate the previous measurements.

**APAP Quantification with LC-MS/MS.** The APAP concentrations in the sweat and saliva samples were measured by LC-MS/MS with a multiple reaction monitoring (MRM) technique. Deuterium-labeled APAP (APAP-$D_4$) was used as the internal standard (IS). For calibration, various concentrations of APAP were spiked into water (Optima LC/MS grade) to make standard solutions of 0, 1, 10, 50, 100, 200, 200, and 500 nM. The sweat and saliva samples were first centrifuged at 14, 000 × *g* for 10 min and 1 μL supernatant was diluted into 498.5 μL water. Then, 0.5 μL 1 μg/mL IS was spiked into 499.5 μL of calibrator or diluted biofluid samples (to reach a final IS concentration of 10 ng/mL). Molecular weight cutoff (MWCO) filtering was used to remove particulate matter from the sample. Accordingly, the IS-spiked samples were loaded into the 10-kDa MWCO centrifugal filters (Amicon Ultra-0.5; Sigma-Aldrich) and centrifuged at 14,000 × *g* for 10 min. The low-molecular-weight filtrate was then transferred into an autosampler vial for APAP quantification.

The HPLC setting followed our previously reported protocol (16). The tandem mass spectrometry was operated in MRM mode recording the following *m/z* transitions: 152.2→110.1 for APAP and 156.2→114.1 for APAP-$D_4$. The declustering potential, entrance potential, collision energy, and collision cell exit potential were optimized at 56 V, 10 V, 23 V, and 6 V for APAP and 71 V, 10 V, 21 V, and 6 V for APAP-$D_4$, respectively. Ionspray voltage and temperature were 5,500 V and 400 °C, respectively. Collision gas, curtain gas, and ion source gas 1 and 2 were set at 4, 30, 30, and 50 psi, respectively.

**Construction of Microfluidic Interface.** The microfluidic interface was created by vertically stacking multiple laser-patterned (VLS2.30; Universal Laser Systems) layers (including PET, double-sided tape, and single-sided laminating sheets). The microfluidic interface consisted of a sweat sampling chamber and a sweat sensing chamber, fluidically connected using a vertical interconnect access. The sweat sampling chamber was created by stacking the double-sided tape layer (with the same dimension as the iontophoretically stimulated area, diameter 28 mm) onto a PET layer. To minimize the dead-sweat volume, a spacer was incorporated in the microfluidic interface, formed by stacking three layers of single-sided laminating sheets. The sweat-sensing chamber was created by stacking PET cover and double-sided tape layers onto the sensor substrate.

**Wireless Electronic Module and Smartwatch Design.** The wireless DPV readout was realized with a custom-developed printed circuit board (PCB). An onboard microcontroller unit (MCU) (Atmega328; Microchip Technology) was utilized to program the applied potential waveform and acquire the readout signal. Specifically, the DPV excitation potential waveform and the cathodic electrical pulse (with the same parameters as the potentiostat measurements) were applied across the working and reference electrodes through a 16-bit digital-to-analog converter (DAC) (DAC8552; Texas Instruments). The current response from the working electrode was acquired as a digital voltage output with the aid of a transfer impedance amplifier (TIA) (LT1462; Linear Technology) and a 12-bit analog-to-digital converter (ADC) (ADS1015; Texas Instruments). The collected current response (through interintegrated circuit protocol, $I^2C$) was then used to construct the differential pulse voltammogram within the MCU. A wireless, bilateral, and real-time communication was achieved between the PCB and the user interface by an onboard Bluetooth module (AMB2621; Wurth Elektronik). Moreover, the MCU communicated with a 1.44-in color thin-film-transistor liquid-crystal display (LCD) screen (SF-TS144C-9082A-N; Shenzhen SAEF Technology) to display the acquired voltammogram. The sensor was connected to the PCB with the aid of a flat, flexible cable (Molex) and a double-sided adhesive anisotropic conductive film (9703; 3M). A single, miniaturized, rechargeable lithium-ion polymer battery with a nominal voltage of 3.7 V was used to power the PCB. A smartwatch case was three-dimensionally (3D)-printed to accommodate all of the functional modules (sensor, microfluidic module, and electronic module) and battery. The developed smartwatch was adhered onto the subject's wrist with the aid of the double-sided adhesive tape.

**On-Body Tracking of APAP Metabolic Profile.** Each iontophoresis test was performed following the same protocol used in the ex situ testing. The devised voltammetric sensing system was then mounted onto the stimulated skin surface to perform DPV measurements (during the course of the sweat secretion). Saliva samples were collected during and in between the sweat analysis. Saliva analysis was performed using circuit-interfaced sensors, similar to the ex situ study. The APAP concentration was calculated by peak information extraction (via analytical framework) and postcalibration.

**Analytical Framework for Peak Height Information Extraction.** To extract the APAP oxidation peak information from the voltammograms, the voltammetric baseline outside the peak region was fitted using the combination of a third-order polynomial and exponential equation in MATLAB (MathWorks), where proper initial values were set for all of the unknown variables:

$$I_{baseline} = a_1 V^3 + a_2 V + a_3 + a_4 \times \exp(a_5 V). \quad [2]$$

The APAP oxidation peak information was extracted by subtracting the estimated baseline from the corresponding raw readout.

**Pharmacokinetic Analysis.** A single-compartment model was used to construct the pharmacokinetic profiles of APAP in sweat and saliva. To fit the captured readouts into the model, first the readouts in the elimination phase were plotted in the semilogarithmic scale and linearly fitted. The preexponential factor *A* was determined as the *y*-intercept of the fitted curve (extrapolated) (53). Then, other parameters ($t_0$, $K_{el}$, and $K_a$) are fitted using the nonlinear least square regression algorithm (MATLAB).

**Institutional Review Board Approval for Human Subject Testing.** The conducted human subject experiments were performed in compliance with the protocols that have been approved by the Institutional Review Board at the University of California, Los Angeles (IRB no. 17-000170). Subjects without recent APAP administration history were recruited. All subjects gave written informed consent before participation in the study.

**Data availability.** All data needed to evaluate the conclusions in the paper are present in the paper and/or *SI Appendix*. Raw data can be accessed through the Open Science Framework at https://osf.io/w3f7g/?view_only=118783b424ee49d59e7b70ea92223020 (DOI: 10.17605/OSF.IO/W3F7G).

**ACKNOWLEDGMENTS.** This work was supported by the S.E.'s startup package provided by the University of California, Los Angeles Henry Samueli School of Engineering and Applied Sciences. Components of this research are supported by the National Science Foundation (Award 1847729), Brain and Behavior Foundation (National Alliance for Research on Schizophrenia & Depression Young Investigator Grant), PhRMA Foundation (Research Starter Grant in Translational Medicine and Therapeutics), and the funding secured by the Preservation of the Force and Family Program at US Special Operations Command (executed as a subaward issued to the University of California, Los Angeles by the Henry M. Jackson Foundation under a cooperative agreement with the Uniformed Services University). We thank Dr. Yu Chen and Gemalene Sunga for their assistance with the standard laboratory instrument test, Ryan Shih for insightful discussion, and Diana Ly for assistance with the concept figure design.

1. K. Pavelić, S. K. Pavelić, M. Sedić, "Personalized medicine: The path to new medicine" in *Personalized Medicine: A New Medical and Social Challenge*, N. Bodiroga-Vukobrat, D. Rukavina, K. Pavelić, G. G. Sander, Eds. (Springer, 2016), pp. 1–19.
2. M. E. G. Bigelow *et al*., Point-of-care technologies for the advancement of precision medicine in heart, lung, blood, and sleep disorders. *IEEE J. Transl. Eng. Health Med.* **4**, 2800510 (2016).
3. J. L. Lenahan *et al*., A drug by any other name: Patients' ability to identify medication regimens and its association with adherence and health outcomes. *J. Health Commun.* **18** (suppl. 1), 31–39 (2013).
4. J.-H. Huang *et al*., Sample sizes in dosage investigational clinical trials: A systematic evaluation. *Drug Des. Devel. Ther.* **9**, 305–312 (2015).
5. J. Jonklaas *et al*.; American Thyroid Association Task Force on Thyroid Hormone Replacement, Guidelines for the treatment of hypothyroidism: Prepared by the american thyroid association task force on thyroid hormone replacement. *Thyroid* **24**, 1670–1751 (2014).
6. D. E. Becker, Pharmacodynamic considerations for moderate and deep sedation. *Anesth. Prog.* **59**, 28–42 (2012).
7. W. Clarke, A. Dasgupta, *Clinical Challenges in Therapeutic Drug Monitoring: Special Populations, Physiological Conditions and Pharmacogenomics*, (Elsevier, 2016).
8. N. Arroyo-Currás *et al*., Real-time measurement of small molecules directly in awake, ambulatory animals. *Proc. Natl. Acad. Sci. U.S.A.* **114**, 645–650 (2017).
9. P. L. Mage *et al*., Closed-loop control of circulating drug levels in live animals. *Nat. Biomed. Eng.* **1**, 70 (2017).
10. S. H. Jang, Z. Yan, J. A. Lazor, Therapeutic drug monitoring: A patient management tool for precision medicine. *Clin. Pharmacol. Ther.* **99**, 148–150 (2016).
11. T. Buclin *et al*., The steps to therapeutic drug monitoring: A structured approach illustrated with imatinib. *Front. Pharmacol.* **11**, 177 (2020).
12. S. Cremers, N. Guha, B. Shine, Therapeutic drug monitoring in the era of precision medicine: Opportunities!. *Br. J. Clin. Pharmacol.* **82**, 900–902 (2016).
13. W. Gao *et al*., Fully integrated wearable sensor arrays for multiplexed in situ perspiration analysis. *Nature* **529**, 509–514 (2016).
14. Y. Zhao *et al*., A wearable freestanding electrochemical sensing system. *Sci. Adv.* **6**, eaaz0007 (2020).
15. L. C. Tai *et al*., Methylxanthine drug monitoring with wearable sweat sensors. *Adv. Mater.* **30**, e1707442 (2018).
16. S. Lin *et al*., Natural perspiration sampling and in situ electrochemical analysis with hydrogel micropatches for user-identifiable and wireless chemo/biosensing. *ACS Sens.* **5**, 93–102 (2020).
17. Y. Yang, W. Gao, Wearable and flexible electronics for continuous molecular monitoring. *Chem. Soc. Rev.* **48**, 1465–1491 (2019).
18. S. Emaminejad *et al*., Autonomous sweat extraction and analysis applied to cystic fibrosis and glucose monitoring using a fully integrated wearable platform. *Proc. Natl. Acad. Sci. U.S.A.* **114**, 4625–4630 (2017).
19. J. Heikenfeld *et al*., Accessing analytes in biofluids for peripheral biochemical monitoring. *Nat. Biotechnol.* **37**, 407–419 (2019).
20. A. Hauke *et al*., Complete validation of a continuous and blood-correlated sweat biosensing device with integrated sweat stimulation. *Lab Chip* **18**, 3750–3759 (2018).
21. V. K. Gupta, R. Jain, K. Radhapyari, N. Jadon, S. Agarwal, Voltammetric techniques for the assay of pharmaceuticals–A review. *Anal. Biochem.* **408**, 179–196 (2011).
22. S. Lin *et al*., Design framework and sensing system for noninvasive wearable electroactive drug monitoring. *ACS Sens.* **5**, 265–273 (2020).
23. C. Jiang *et al*., Antifouling strategies for selective *in vitro* and *in vivo* sensing. *Chem. Rev.* **120**, 3852–3889 (2020).
24. W. Yantasee *et al*., Electrochemical sensors for the detection of lead and other toxic heavy metals: The next generation of personal exposure biomonitors. *Environ. Health Perspect.* **115**, 1683–1690 (2007).
25. S. Suwal, A. Doyen, L. Bazinet, Characterization of protein, peptide and amino acid fouling on ion-exchange and filtration membranes: Review of current and recently developed methods. *J. Membr. Sci.* **496**, 267–283 (2015).
26. C. Rodriguez-Emmenegger, M. Houska, A. B. Alles, E. Brynda, Surfaces resistant to fouling from biological fluids: Towards bioactive surfaces for real applications. *Macromol. Biosci.* **12**, 1413–1422 (2012).
27. J. P. Glynn, W. Bastain, Salivary excretion of paracetamol in man. *J. Pharm. Pharmacol.* **25**, 420–421 (1973).
28. D. T. Lowenthal, S. Oie, J. C. Van Stone, W. A. Briggs, G. Levy, Pharmacokinetics of acetaminophen elimination by anephric patients. *J. Pharmacol. Exp. Ther.* **196**, 570–578 (1976).
29. A. M. Larson *et al*.; Acute Liver Failure Study Group, Acetaminophen-induced acute liver failure: Results of a United States multicenter, prospective study. *Hepatology* **42**, 1364–1372 (2005).
30. A. J. Bard, L. R. Faulkner, J. Leddy, C. G. Zoski, *Electrochemical Methods: Fundamentals and Applications*, (Wiley, New York, 1980).
31. S. P. Kounaves, "Voltammetric techniques" in *Handbook of Instrumental Techniques for Analytical Chemistry*, F. A. Settle, Ed. (Prentice Hall, 1997), pp. 709–726.
32. S. Ranganathan, T.-C. Kuo, R. L. McCreery, Facile preparation of active glassy carbon electrodes with activated carbon and organic solvents. *Anal. Chem.* **71**, 3574–3580 (1999).
33. L. Hu *et al*., Dominant factors governing the electron transfer kinetics and electrochemical biosensing properties of carbon nanofiber arrays. *ACS Appl. Mater. Interfaces* **8**, 28872–28879 (2016).
34. K. Asai, T. A. Ivandini, M. M. Falah, Y. Einaga, Surface termination effect of boron-doped diamond on the electrochemical oxidation of adenosine phosphate. *Electroanalysis* **28**, 177–182 (2016).
35. K. Asai, T. A. Ivandini, Y. Einaga, Continuous and selective measurement of oxytocin and vasopressin using boron-doped diamond electrodes. *Sci. Rep.* **6**, 32429 (2016).
36. E. Popa, H. Notsu, T. Miwa, D. A. Tryk, A. Fujishima, Selective electrochemical detection of dopamine in the presence of ascorbic acid at anodized diamond thin film electrodes. *Electrochem. Solid-State Lett.* **2**, 49 (1998).
37. N. Yang *et al*., Conductive diamond: Synthesis, properties, and electrochemical applications. *Chem. Soc. Rev.* **48**, 157–204 (2019).
38. J. V. Macpherson, A practical guide to using boron doped diamond in electrochemical research. *Phys. Chem. Chem. Phys.* **17**, 2935–2949 (2015).
39. M. Hupert *et al*., Conductive diamond thin-films in electrochemistry. *Diamond Relat. Mater.* **12**, 1940–1949 (2003).
40. K. Muzyka *et al*., Boron-doped diamond: Current progress and challenges in view of electroanalytical applications. *Anal. Methods* **11**, 397–414 (2019).
41. K. Aoki, K. Tokuda, H. Matsuda, Theory of differential pulse voltammetry at stationary planar electrodes. *J. Electroanal. Chem. Interfacial Electrochem.* **175**, 1–13 (1984).
42. A. P. P. Eisele, D. N. Clausen, C. R. T. Tarley, L. H. Dall'Antonia, E. R. Sartori, Simultaneous square-wave voltammetric determination of paracetamol, caffeine and orphenadrine in pharmaceutical formulations using a cathodically pretreated boron-doped diamond electrode. *Electroanalysis* **25**, 1734–1741 (2013).
43. A. M. Santos, F. C. Vicentini, P. B. Deroco, R. C. Rocha-Filho, O. Fatibello-Filho, Square-wave voltammetric determination of paracetamol and codeine in pharmaceutical and human body fluid samples using a cathodically pretreated boron-doped diamond electrode. *J. Braz. Chem. Soc.* **26**, 2159–2168 (2015).
44. V. Bernal, A. Erto, L. Giraldo, J. C. Moreno-Piraján, Effect of solution pH on the adsorption of paracetamol on chemically modified activated carbons. *Molecules* **22**, 1032 (2017).
45. J. Wang, R. P. Deo, S. Thongngamdee, B. Ogorevc, Effect of surface-active compounds on the stripping voltammetric response of bismuth film electrodes. *Electroanalysis* **13**, 1153–1156 (2001).
46. B. Hoyer, T. M. Florence, G. E. Batley, Application of polymer-coated glassy carbon electrodes to the direct determination of trace metals in body fluids by anodic stripping voltammetry. *Anal. Chem.* **59**, 1608–1614 (1987).
47. Y. Huang, A. Hara, C. Terashima, A. Fujishima, M. Takai, Protein adsorption behavior on reduced graphene oxide and boron-doped diamond investigated by electrochemical impedance spectroscopy. *Carbon* **152**, 354–362 (2019).
48. V. A. LeGrys, *Sweat Testing: Sample Collection and Quantitative Analysis: Approved Guideline*, (NCCLS, 1994).
49. W. Lu, S. Zhao, M. Gong, L. Sun, L. Ding, Simultaneous determination of acetaminophen and oxycodone in human plasma by LC-MS/MS and its application to a pharmacokinetic study. *J. Pharm. Anal.* **8**, 160–167 (2018).
50. H. Lin *et al*., A rapid and low-cost fabrication and integration scheme to render 3D microfluidic architectures for wearable biofluid sampling, manipulation, and sensing. *Lab Chip* **19**, 2844–2853 (2019).
51. G. Ogata *et al*., A microsensing system for the in vivo real-time detection of local drug kinetics. *Nat. Biomed. Eng.* **1**, 654–666 (2017).
52. R. Kiran, E. Scorsone, P. Mailley, P. Bergonzo, Quasi-real time quantification of uric acid in urine using boron doped diamond microelectrode with in situ cleaning. *Anal. Chem.* **84**, 10207–10213 (2012).
53. M. A. Hedaya, "Extravascular routes of drug administration" in *Basic Pharmacokinetics*, S. S. Jambhekar, P. J. Breen, Eds. (Pharmaceutical Press, London, 2012), Vol. 2, pp. 105–126.
54. M. T. Borin, J. W. Ayres, Single dose bioavailability of acetaminophen following oral administration. *Int. J. Pharm.* **54**, 199–209 (1989).